# Highly Dispersive Photonic Crystal Waveguides and their Applications in Optical Modulators and True-Time Delay Lines

Yongqiang Jiang[1], Tao Ling[1], Lanlan Gu[1], Wei Jiang[1,2], Xiaonan Chen[1], Ray T. Chen[1,*]
[1]Microelectronic Research Center, Department of Electrical and Computer Engineering, The University of Texas at Austin, Austin, TX 78758, USA
[2]Omega Optics, Austin, TX 78758, USA
* Email: chen@ece.utexas.edu

## ABSTRACT

An ultra-compact silicon electro-optic modulator was experimentally demonstrated based on highly dispersive silicon photonic crystal (PhC) waveguides. Modulation operation was demonstrated by carrier injection into an 80 μm-long silicon PhC waveguide of a Mach-Zehnder interferometer (MZI) structure. The π phase shift driving current, $I_\pi$, across the active region is as low as 0.15 mA, which is equivalent to a $V_\pi$ of 7.5 mV when a 50 Ω impedance-matched structure is applied. The modulation depth is 92%. Highly dispersive PhC fibers were previously proposed to reduce the payload of true-time delay (TTD) modules for phased-array antenna (PAA) systems. The payload reduction factor is proportional to the enhanced dispersion of highly dispersive PhC fibers. An ultra-large dispersion of $-1.1\times10^4$ ps/nm·km with the full width at half maximum (FWHM) of 40 nm was numerically simulated from a dual core PhC fibers. The payload reduction factor of the TTD module is as high as 110 compared to that using conventional dispersion compensation fibers (D = -100 ps/nm·km).

**Keywords**: Photonic crystal (PhC), optical modulator, Mach-Zehnder interferometer (MZI), group velocity dispersion, plasma dispersion effect, true-time delay (TTD), phased array antenna (PAA)

## I. INTRODUCTION

Photonic crystals (PhCs) are a class of artificial optical materials with periodic dielectric structures, which result in unusual optical properties. PhCs now show promise to be a key platform for future optical integrated circuits [1-3]. Due to the unique properties of PhCs, the size of many optical components is anticipated to be greatly reduced by employing PhC structures, such as photonic crystal waveguides. In the most commonly employed configuration, a photonic crystal waveguide is formed by introducing a line defect into a two-dimensional (2D) PhC slab [4-15]. In such PhC waveguides, light is confined by a combination of in-plane PBG confinement and vertical index guiding. A size reduction mechanism based on slow group velocity in photonic crystal waveguides has been discussed for an array of optical devices [15]. Notomi *et al.* firstly demonstrated low group velocity and high group velocity dispersion using silicon PhC slab line defect waveguides [8]. Several other groups also demonstrated this effect in both line-defect and coupled-cavity PhC waveguides [12-15].

In the context of microelectronics, silicon has been the optimal material for microelectronics for a long time, but it has only relatively recently been considered as an option for photonics [16-18]. Silicon is transparent in the range of optical telecommunication wavelengths, 1.3 μm and 1.55 μm, and has high refractive index that allows for the fabrication of high-index-contrast nano-photonic structures. In addition, as silicon photonics technology is compatible with conventional complementary metal-oxide-semiconductor (CMOS) processing, monolithic integration of silicon photonic devices with advanced electronics on a single silicon substrate becomes possible. Optical modulators are pivotal components in silicon based optoelectronic integrated circuits. Most silicon electro-optic modulators are based on plasma dispersion effect, through which carrier concentration perturbation results in refractive index change [16-18]. There are a number of ways to vary the carrier concentration in silicon including carrier injection and capacitive coupling though the metal-oxide-semiconductor (MOS) field effect [19-22]. For broadband

optical intensity modulators, the silicon Mach-Zehnder Interferometer (MZI) structure that converts a phase modulation into an intensity modulation is widely used [19-22]. However, conventional silicon MZI modulators are based on rib waveguides, which usually need one-half to several millimeters to achieve the required phase shift in MZI structures [19-22]. The reason is that propagation constant perturbation, $\Delta\beta$, is fairly low, thus requiring larger rib waveguide length, $L$, to achieve required phase shift, $\Delta\phi = \Delta\beta \times L$.

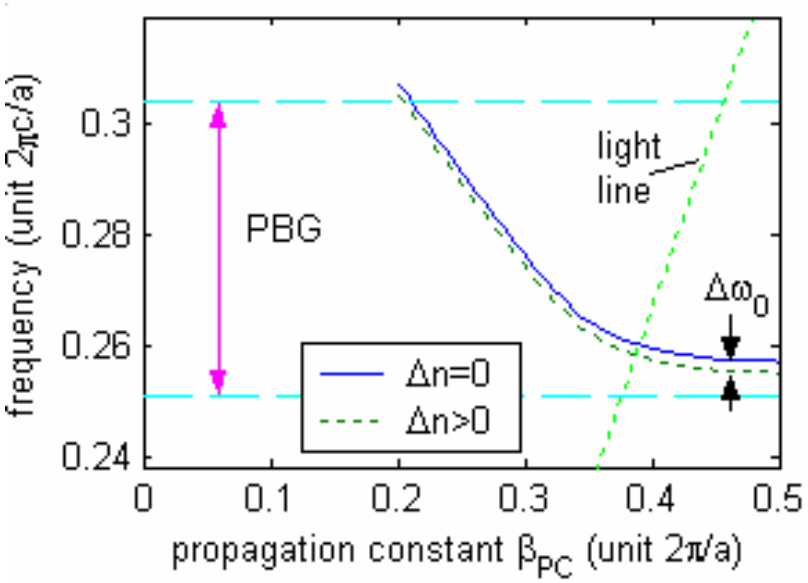


Fig. 1. Dispersion relation of a guide mode of a photonic crystal waveguide

The extraordinary dispersion of photonic crystal (PhC) waveguides offers an unprecedented opportunity for developing ultra-compact MZI modulators. Consider a typical dispersion relation for a PhC waveguide mode shown in Fig. 1. If the refractive index of the waveguide core material (*i.e.* silicon) varies by an amount of $\Delta n$, the dispersion curve will shift vertically by an amount $\Delta\omega_o$. As theoretically explained by Soljacic et al. [15], for a fixed frequency of light, the propagation constant $\beta_{PC}$ of PhC waveguide changes as $\Delta\beta_{PC} = \frac{d\beta_{PC}}{d\omega}\Delta\omega_0$, which grows significantly whenever the group velocity $\frac{d\omega}{d\beta_{PC}}$ approaches zero, e.g. on the right-most segment of dispersion curve in Fig. 1. Such an extraordinary growth of $\Delta\beta_{PC}$ directly leads to a significant enhancement of phase modulation efficiency because the phase change is related to the change of propagation constant and waveguide length $L$ as $\Delta\phi_{PC} = \Delta\beta_{PC} \times L$. One can easily enhance $\Delta\beta_{PC}$ by more than 100 times using a photonic crystal waveguide. Therefore, a 100 times shorter PhC waveguide can produce the same phase change as a long conventional waveguide. The short device length is a benign feature for many other device performance considerations. The optical modulator device has a short PhC waveguide of a few tens of microns in length, which promises a low propagation loss. The power dissipation of the modulator is also expected to be one to two orders of magnitude lower owing to the much shorter electrode length.

Photonic crystals can find applications not only in optical modulators but also in optical true-time delay (TTD) lines for phased-array antenna (PAA) systems. PAAs are a promising technology in modern civilian and military communication and targeting systems. However, the application of phased-array antennas is limited by conventional, intrinsically narrow-band electrical phase trimmers. The narrow-band phase trimmer technique also introduces beam squint. Since the 1990's, there has been growing interest in optical TTD techniques with the exciting features of wide bandwidth, reduced system weight and size, and low electromagnetic interference when compared with electrical TTD techniques [23-27]. However, most of the optical TTD techniques require a large number of precisely time-delay matched optical elements such as lasers and optical delay segments. This usually results in a complex system design that may also suffer from large power losses, specialized component needs, instability, or inability to easily scale to real-

world two-dimensional (2-D) arrays. Esman *et al* proposed a fiber-optic TTD technique using conventional dispersion compensating fiber (DCF) to meet these requirements [24]. However, the dispersion parameter D, of conventional DCF is of fairly small magnitude (D = -100 ps/nm·km), and therefore long fiber lengths are still needed in the TTD module to get the required time delay. If the fiber group velocity dispersion is increased, the total fiber length will be decreased proportionally.

Conventional single-mode fibers (SMFs), which are based on weakly guiding structures with doped silica, can be tailored to slightly increase the dispersion by increasing the refractive index difference between the core and cladding [28]. However, the dispersion cannot be changed significantly because of the small index variation across the transverse cross section of the fiber from doping. This shortcoming can be overcome by the employment of highly dispersive PhC fibers. PhC fibers have generated a lot of interest due to their unusual and attractive properties [28-35]. They are usually made of silica or polymer materials with a regular hexagonal array of sub-micrometer-sized air holes running along the axis of the fiber as a cladding. A defect, usually one or multiple missing holes, acts as core. The dispersion of the PhC fibers can be flexibly tailored by tuning the pitch of the periodic array, the hole diameter and the doping concentration of the core. Jiang *et al* [36-37] demonstrated to use highly dispersive PhC fibers (D = -600 ps/nm·km) to reduce the payload of TTD modules for PAA system. The payload reduction factor is proportional to the enhanced dispersion of highly dispersive PhC fibers. By designing PhC fibers to enhance the dispersion, the TTD payload can be further reduced.

## II. ULTRA-COMPACT SILICON PHOTONIC CRYSTAL WAVEGUIDE MODULATOR

A schematic of a silicon MZI modulator is shown in Fig. 2. The MZI modulator is composed of PhC waveguides, rib waveguides, Y-junctions, electrodes, and electrode pads. PhC waveguides are used in both arms of the MZI modulator to ensure the two arms have the same optical loss and dispersion; otherwise the modulation depth may suffer a reduction.

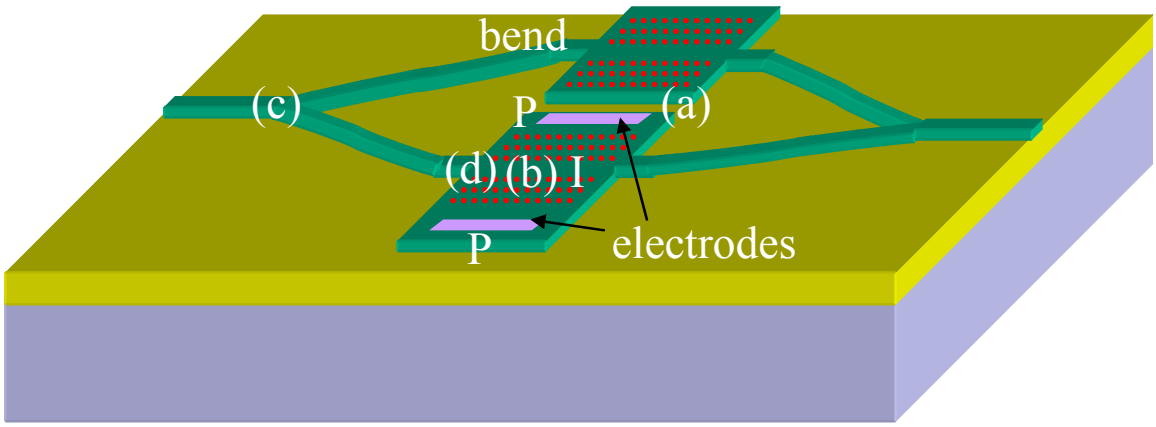


Fig. 2. Schematic diagram of the silicon Mach-Zehnder PhC modulator. Electrode structure of the modulator with PIP regions indicated.

PhC waveguides of the MZI modulator are designed fabricated and characterized [38]. A line-defect (W-1) PhC waveguide can be easily generated by removing a single row of air holes from a 2-D PhC slab. The dispersion diagram of PhC waveguides is calculated using the 3-D fully vectorial plane-wave expansion (PWE) method [39]. The slab is fabricated on a silicon-on-insulator (SOI) wafer. The thickness of the silicon core layer is $t$ = 215 *nm*. The top cladding is air and the bottom cladding is a buried oxide layer of 2 $\mu m$ thick. The pitch size of the hexagonal PhC lattice is $a$ = 400 *nm*. The normalized air hole diameter is designed to be $d/a$ = 0.53.

To fabricate the ultra-compact silicon MZI modulator, the designed PhC waveguides, rib waveguides, and Y-junctions are first fabricated on a SOI wafer. A PIP structure is formed by an implantation of boron at 25 keV with a peak concentration of $2\times10^{17}$ $cm^{-3}$ into an N-type Si substrate with the doping concentration of $1\times10^{14}$ $cm^{-3}$. Medici simulation tool shows the P-I-P diode injects holes only. The PIP I-V

curve is experimentally confirmed for both forward and reverse biases. Note that the N-type Si substrate with $1\times10^{14}$ $cm^{-3}$ doping concentration is defined as intrinsic [40]. The PhC and Si rib waveguide structures are patterned with E-beam resist ZEP-520A by E-beam lithography (Jeol JBX6000). After developing the resist, the patterns are transferred to a 57 nm oxide mask layer by reactive ion etching (RIE) using $CHF_3$. Then the E-beam resist residue is removed by plasma ashing in oxygen. Using the oxide layer as a hard mask the patterns are transferred to the silicon core layer by a HBr and $Cl_2$ RIE process. Post-etching oxidation at 850°C is implemented for about 1 minute. The post-etching oxidation forms an additional 5~7nm oxide layer, resulting in the sidewalls of the air-holes being significantly smoother than the original surface after dry etching [38]. Extensive experimentation with various processes is conducted to determine the optimized process parameters. A proper pre-offset of the hole size in e-beam pattern design is used so that the hole size can be controlled with an accuracy of 5%. After the silicon photonic crystal waveguides and rib waveguides are fabricated, the regions for the aluminum electrodes and pads are patterned by a conventional photolithography mask aligner, followed by metal deposition and metal liftoff. Aluminum electrodes and pads are then sintered to form ohmic contacts with the top silicon layer. The SEM picture of the final structure is shown in Fig. 3, with the corresponding sections marked in Fig. 2.

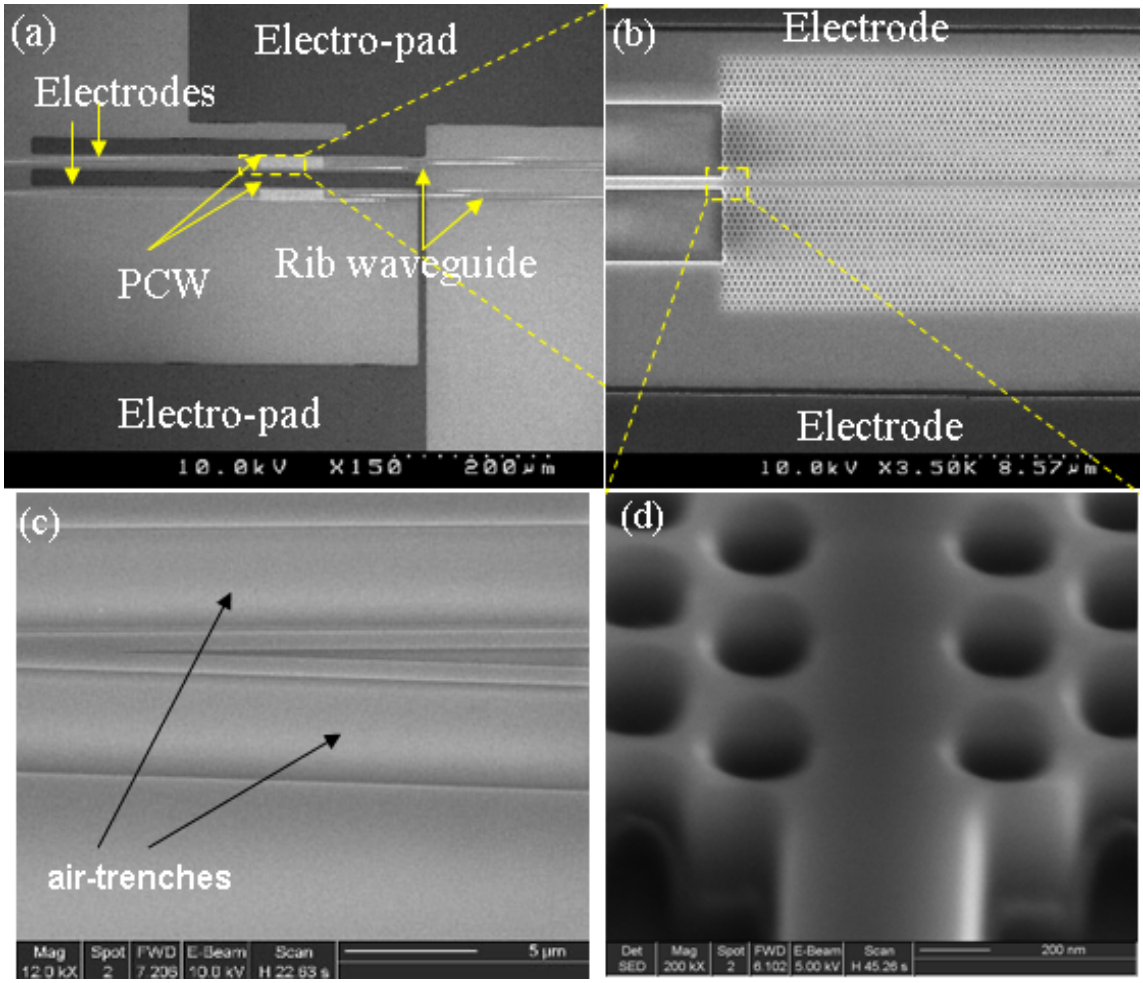


Fig. 3. SEM pictures of the silicon PhC modulator: (a) overview picture of the modulator. (b) PhC waveguide with two electrodes. (c) Y-junction. (d) Magnified PhC waveguide based on a triangular lattice with lattice constant $a$ = 400nm, hole diameter $d$ = 210 nm, and top Si thickness $t$ = 215 nm, buried oxide (BOX) $SiO_2$ thickness of 2 µm.

For the optical measurement, we introduce a silicon rib waveguide bend [41], which shifts the output silicon rib waveguide by at least 600 µm and significantly suppresses the stray light collected by the output fiber. The measurement is performed on a fully-automated Newport Photonics Alignment/Packaging

Station. Two lensed fibers are manipulated by two automated 5-axis stages, which are controlled by a computer to precisely align the fibers with the rib waveguides. The input lensed fiber is aligned for the transverse electrical (TE) mode with the electric field vector primarily in plane. The TE polarized light is used for all the measurement presented here. The propagation loss of passive photonic crystal waveguides fabricated with the aforementioned processing sequence is around 6 dB/mm [38]. Note that the waveguides fabricated without post-etching oxidation typically have propagation loss over 20 dB/mm, which manifests the advantage of oxidation.

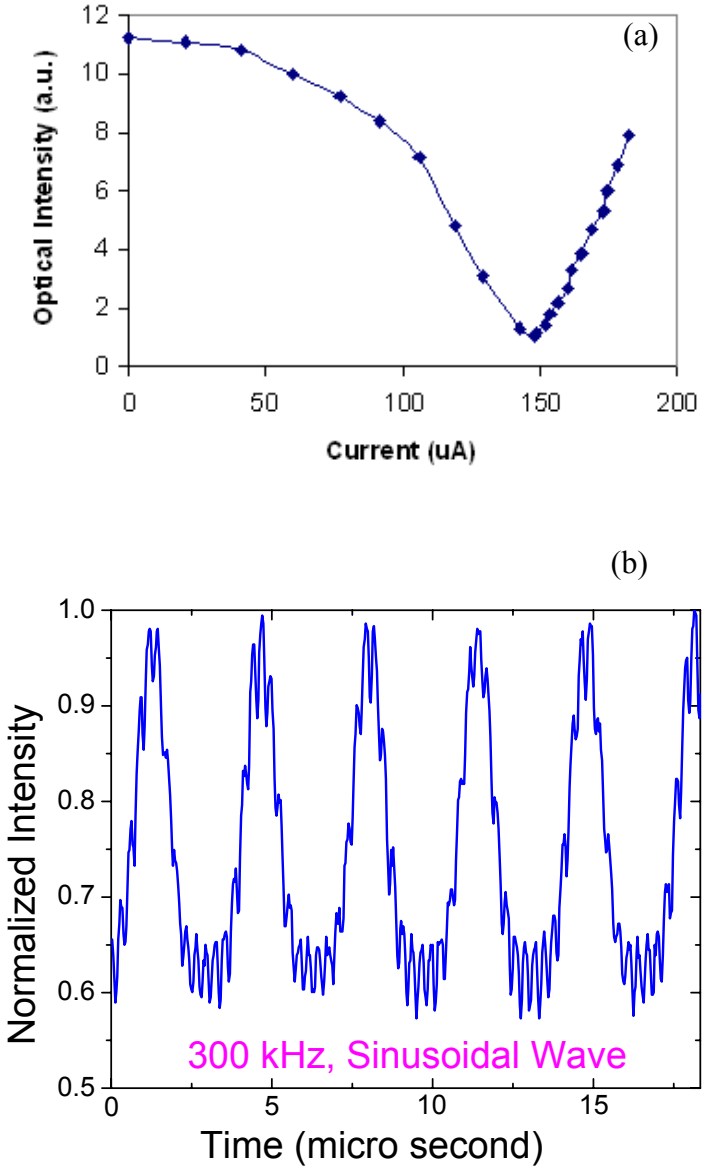


Fig. 4. Modulation characteristics (a) Intensity vs. injection current, 92% modulation depth is achieved at 0.15mA; (b) Modulation curve of 300 kHz sinusoidal wave with peak current of 0.11 mA.

We investigate the modulation performance of the fabricated modulators. We characterize the modulation depth and the minimum current needed for phase shift of $\pi$, $I_\pi$, of our silicon MZI modulator operating at 1567 nm. We have measured the transmission spectra which confirm that 1567 nm falls into the bandedge of the transmission spectra. The optical output intensity against drive current is shown in Fig.

4(a). The modulation depth of 92% is clearly seen in Fig. 4(a). The modulated signal is displayed in Fig. 4(b) with sinusoidal input signal at 300 kHz. The π radian drive current, $I_\pi$, is a typical measure of the quality of such MZI modulator devices. The $I_\pi$ of our silicon MZI modulator is as low as 0.15 mA compared to several mA in conventional MZI modulator devices [17-18], which shows the high quality of our MZI modulator device. With a 50 Ω impendence matched lumped electrode structure, it is equivalent to a $V_\pi$ of 7.5 mV. The length of the modulator is reduced to 80 μm compared to several millimeters for the modulators using silicon rib waveguides in MZI structures [15-16], due to the extraordinary dispersion of the PhC waveguide. All of these prove the proposed advantages of using PhC waveguide instead of conventional rib waveguide mentioned above. The thermo-optic effect is excluded as a mechanism for phase shift, because the power dissipation $I^2R$ is very low, and the subsequent temperature rise of the waveguide only less than 0.3 $^oC$.

## III. HIGHLY DISPERSIVE PHOTONIC CRYSTAL FIBERS FOR TRUE-TIME DELAY LINES

A 1×N TTD module is proposed using the highly dispersive PhC fiber delay lines, as shown in Fig. 5 [36-37]. The lengths of the highly dispersive PhC fibers are L, L·(N-2)/(N-1), L·(N-3)/(N-1), … , L·2/(N-1), L·1/(N-1), and 0, respectively. Each delay line has the same nominal group delay at the central tuning wavelength $\lambda_0$ but with slightly different net dispersion. This can be constructed by connecting varying lengths of highly dispersive PhC fibers and non-dispersive fibers (D < 3 ps/nm·km). The relative delay of the signals among the delay lines can thus be changed by tuning the optical wavelength. At the central tuning wavelength $\lambda_0$ all the time delays are matched by trimming the non-dispersive fibers. Thus, at $\lambda_0$ the main antenna beam will be directed broadside. At wavelengths deviating from $\lambda_0$, each of the fiber delay lines generates a time delay proportional to its dispersion parameter, D, and the highly dispersive PhC fiber length, resulting in a phase change to steer the main antenna radiation beam.

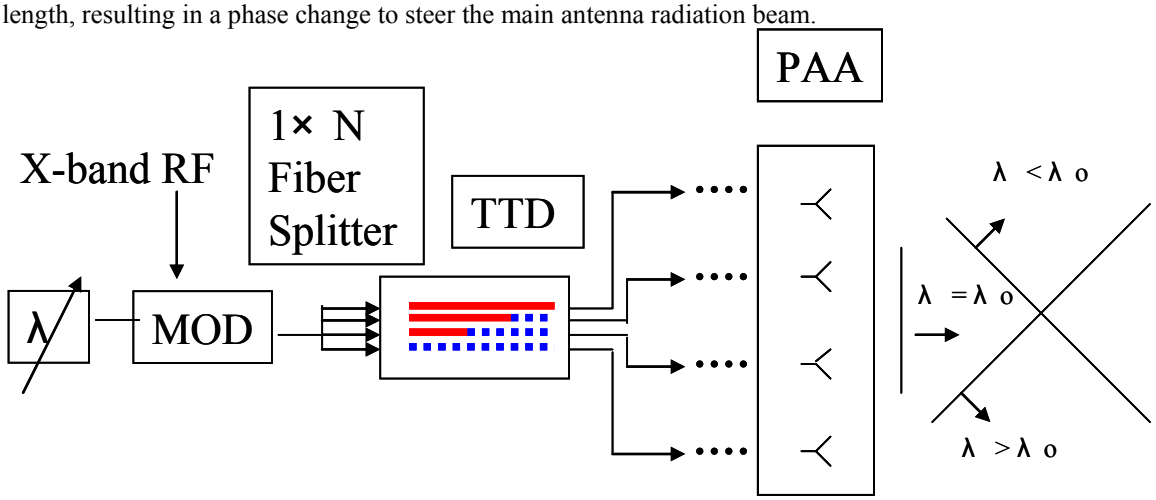


Fig. 5. Highly dispersive PhC fiber enhanced wavelength continuous tunable PAA system structure. (Dashed line: highly dispersive PhC fibers; solid line: Non-dispersive fibers; MOD: modulator)

The transverse section of PhC fibers usually consists of a regular hexagonal array of microscopic holes in silica glass that extends along the entire fiber length. There are one or several defects (missing holes with or without doping) located in the center of the regular hexagonal structure. We use a dual-core PhC fibers design to achieve high dispersion. The inner core is a missing air hole, and the outer core is the 4$^{th}$ concentric ring of air holes, as shown in Fig. 6. This dual-core PhC fibers can support two supermodes, which are analogous to the two supermodes of a directional coupler [36-37]. These modes are nearly phase matched at 1550 nm. Close to the phase matching wavelength, the mode index of the PhC fibers changes rapidly due to strong coupling between the two individual modes of the inner core and outer core. Due to strong refractive index asymmetry between the two cores, there is a rapid change in the slope of the wavelength variation of the fundamental mode index. This leads to a large dispersion around 1550 nm. The air hole structure helps not only to guide the mode, but also to increase the dispersion value.

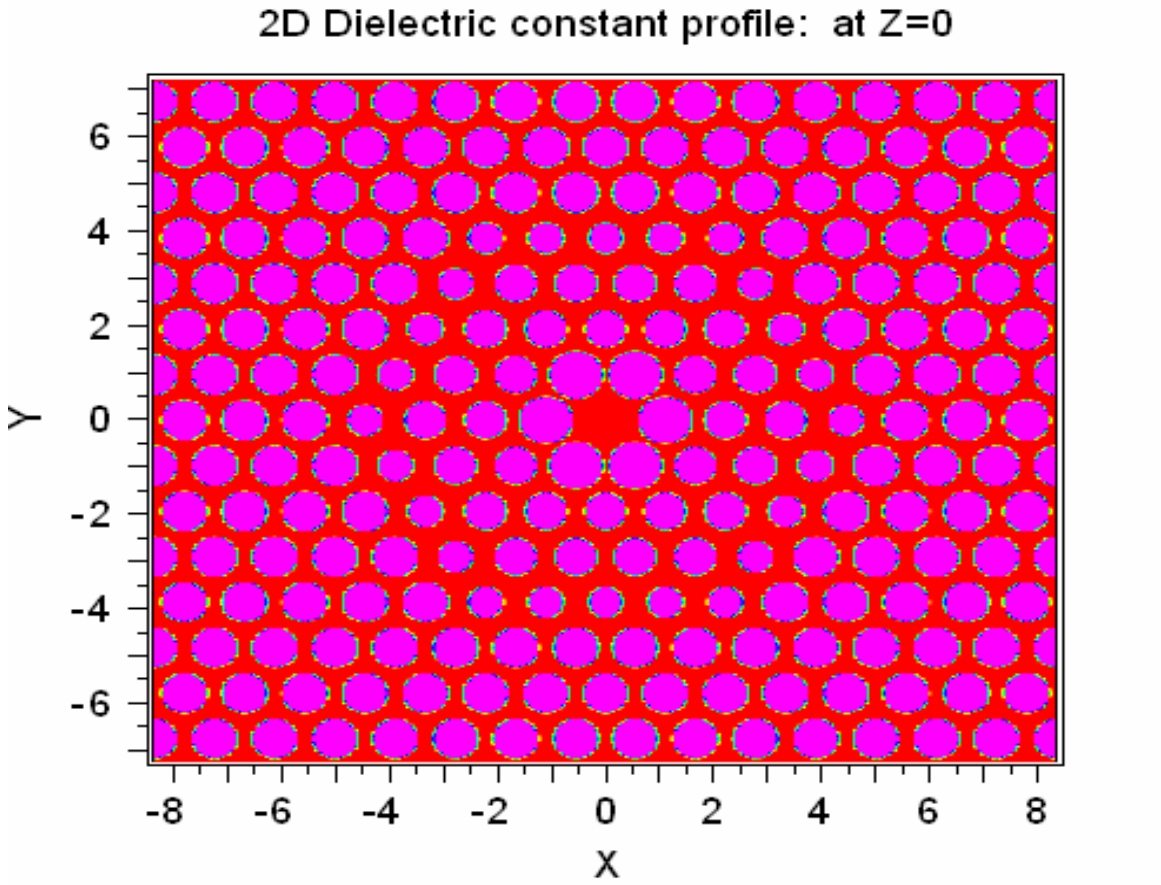


Fig. 6. Transverse cross section of highly dispersive PhC fibers (Period $\Lambda$=1.113 μm, 1st ring $d_1/\Lambda$ = 0.90, 2nd and 3rd rings $d_{2\text{-}3}/\Lambda$ = 0.70, 4th ring $d_4/\Lambda$ = 0.59, other rings $d_{outside}/\Lambda$ =0.76, the red region is silica glass with refractive index n = 1.444, the pink region is air with n = 1.000)

The dispersion of PhC fibers can be calculated using the full vectorial plane-wave expansion (PWE) method, which is fast and accurate compared to other methods. We simulate the PhC fibers by using Bandsolve™ software that is based on full vectorial PWE. The group velocity dispersion or simply the dispersion parameter D(λ) of the guided mode of the PhC fibers can be directly calculated from the modal effective index $n_{eff}(\lambda)$ of the fundamental mode over a range of wavelengths

$$D(\lambda) = -\frac{\lambda}{c}\frac{d^2 n_{eff}(\lambda)}{d\lambda^2} \quad (1)$$

where the effective refractive index of the mode is given by $n_{eff} = \beta[\lambda, n_m(\lambda)]/k_0$, where β is the propagation constant and $k_0$ is the free-space wave number. The dispersion parameter, D(λ), of PhC fibers is strongly related to the structure and refractive index perturbation, and can thus be changed to achieve the desired characteristics. In our design, we use different period Λ, and hole diameters $d_1$, $d_2$, $d_3$, $d_4$, $d_{outside}$, as shown in Fig. 6, to tune the dispersion. By tuning these parameters, we can obtain the large dispersion parameter, D, value that we desire. The simulated guided modes are shown in Fig. 7. Fig. 8 shows the simulated effective index vs. wavelength. Fig. 9 shows the theoretical simulation results of highly dispersive PhC fibers with differing parameters using the full vectorial PWE method. The payload reduction factor is proportional to the enhanced dispersion of highly dispersive PhC fibers. An ultra-high dispersion of $-1.1\times10^4$ ps/nm·km at 1550 nm with the full width at half maximum (FWHM) of 40 nm is obtained. The payload reduction factor of the TTD module is as high as 110 compared to that using conventional dispersion compensation fibers (D = -100 ps/nm·km).

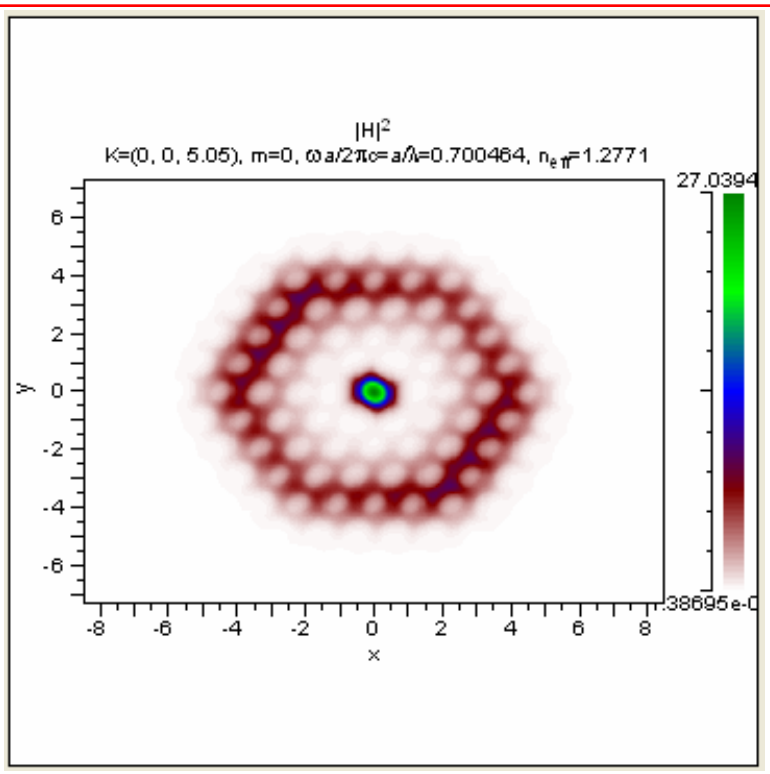


Fig. 7. Simulated guided mode of highly dispersive photonic crystal fibers

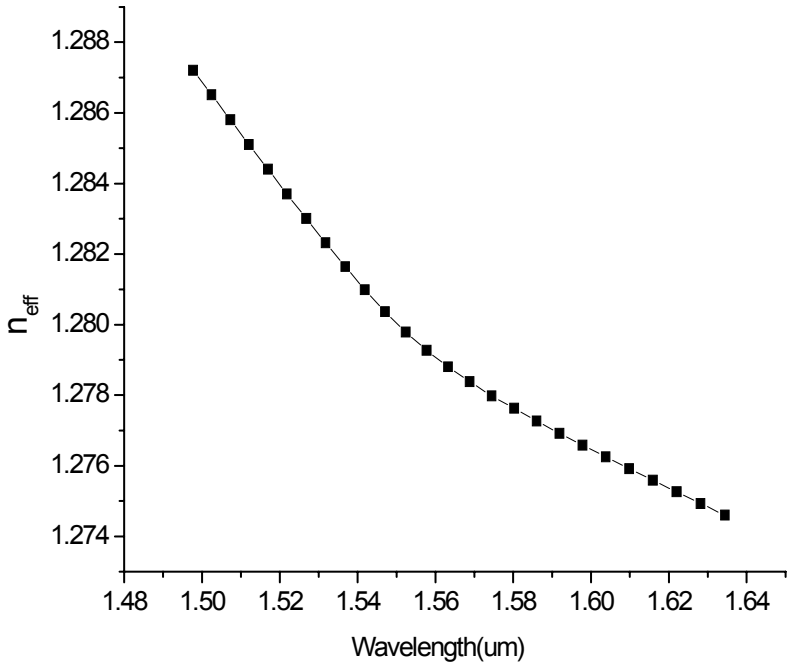


Fig. 8. Simulated effective index vs. wavelength of highly dispersive photonic crystal fibers

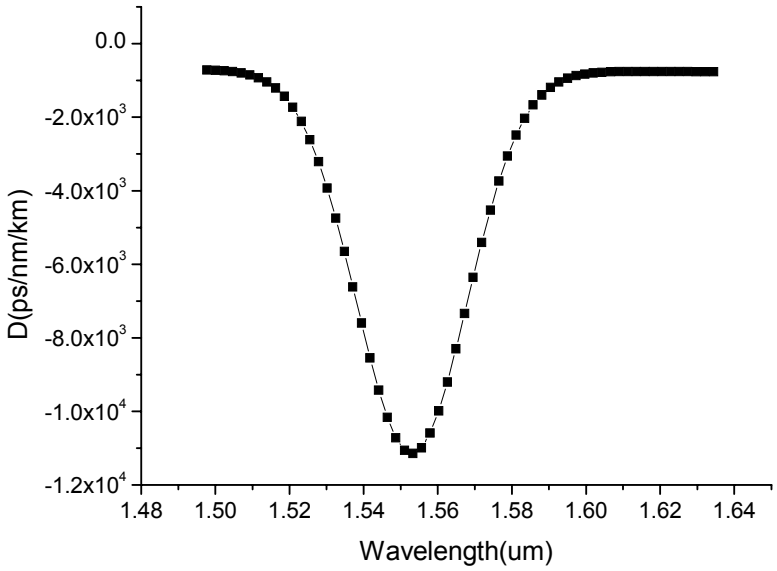


Fig. 9. Simulated dispersion vs. wavelength of highly dispersive photonic crystal fibers

## IV. CONCLUSION

In conclusion, we designed, fabricated, and characterized an ultra-compact silicon electro-optic modulator based on silicon photonic crystal waveguides with a hexagonal lattice of air holes. Modulation operation was demonstrated by carrier injection into an 80 μm-long silicon photonic crystal waveguide. The modulation depth is over 92%. The $I_\pi$ is as low as 0.15 mA. Further improvement in device performance is expected by optimizing the electrode design and reducing the contact resistance. We also numerically simulated an ultra-high dispersion of $-1.1\times10^4$ ps/nm·km with the full width at half maximum (FWHM) of 40 nm from a dual core PhC fibers. The payload reduction factor of the TTD module was as high as 110 compared to that using conventional dispersion compensation fibers (D = -100 ps/nm·km).

## ACKNOWLEDGMENTS

This research is supported in part by AFOSR and DARPA. Technical advice from Drs. Gernot Pomrenke and Richard Soref is acknowledged. The authors are indebted to the State of Texas and SEMATECH for support under the AMRC program. The devices were fabricated at UT MRC with nanofabrication facilities partially supported under NSF's NNIN program. We thank the CNM of UT Austin, Welch Foundation and SPRING for partial support of the Dual Beam FIB/SEM usage. We appreciate Dr. J. R. Cao of the University of Southern California and Dr. B.L. Miao of the University of Delaware for fruitful discussions.

## REFERENCES

[1] E. Yablonovitch, Phys. Rev. Lett. **58**, 2059 (1987)
[2] S. John, Phys. Rev. Lett. **58**, 2486 (1987)
[3] J.D. Joannopoulos, R.D. Meade, J.N. Winn, *Photonic Crystals*, Princeton University Press (1995)
[4] S.G. Johnson, S. Fan, P.R. Vileneuve, J.D. Joannopoulos, L.A. Kolodziejski, Phys. Rev. B **60**, 5751 (1999)
[5] M. Tokushima, H. Kosaka, A. Tomita, and H. Yamada, App. Phys. Lett. **76**, 952 (2000)

[6] M. Loncar, D. Nedeljkovic, T. Doll, J. Vuckovic, and A. Scherer, "Waveguiding in planar photonic crystals," Appl. Phys. Lett. **77**, 1937 (2000)
[7] S. J. McNab, N. Moll, and Y. A. Vlasov, Opt. Express **11,** 2927 (2003)
[8] M. Notomi, K. Yamada, A. Shinya, J. Takahashi, C. Takahashi, I. Yokohama, Phys. Rev. Lett. **87**, 253902 (2001)
[9] T. Baba, D. Mori, K. Inoshita, Y. Kuroki, IEEE J. Selected Topics Quantum Electronics **10**, 484 (2004)
[10] W. Bogaerts, R. Baets, P. Dumon, V. Wiaux, S. Beckx, D. Taillaert, B. Luyssaert, J. Van Campenhout, P. Bienstman, D. Van Thourhout, J. Lightwave Technology **23**, 401 (2005)
[11] B.L. Miao, C.H. Chen, S.Y. Shi, J. Murakowski, D. W. Prather, IEEE Photonics Technology Letters **16**, 2469 (2004)
[12] T. Asano, K. Kiyota, D. Kumamoto, B.S. Song, S. Noda, App. Phys. Lett. **84**, 4690 (2004)
[13] D. Mori, T. Baba, App. Phys. Lett. **85**, 1101 (2004)
[14] T.J. Karle, Y.J. Chai, C.N. Morgan, I.H. White, T.F. Krauss, J. lightwave technology **22**, 514 (2004)
[15] M. Soljacic, J.D. Joannopoulos, Nature materials **3**, 211 (2004); M Soljacic, S. G. Johnson, S. Fan, M. Ibanescu, E. Ippen, J. D. Joannopoulos, J. Opt. Soc. Am. B **19**, 2052 (2002)
[16] R. A. Soref, B. R. Bennett, IEEE J. Quantum Electron. **QE-23**, 123 (1987)
[17] R. A. Soref, Proc. SPIE, **5730**, 19 (2005)
[18] G. Reed, A. P. Knights, *Silicon Photonics, an introduction*, John Wiley & Sons (2004)
[19] A. Liu, R. Jones, L. Liao, D. Samara-Rubio, D. Rubin, O. Cohen, R. Nicolaescu, and M. Paniccia., Nature **427**, 615 (2004)
[20] L. Liao, D. Samara-Rubio, M. Morse, A. Liu, D. Hodge, D. Rubin, U. D. Keil, and T. Franck, Opt. Express **13**, 3129 (2005)
[21] C.Z. Zhao, G.Z. Li, E.K. Liu, Y. Gao, and X.D. Liu, Appl. Phys. Lett. **67**, 2448 (1995)
[22] G.V. Treyz, P.G. May and J.M. Halbout, Appl. Phys. Lett., **59**, 771 (1991)
[23] W. Ng, A. A. Walston, G. L. Tangonan, J. J. Lee, I. L. Newberg, and N. Bernstein, IEEE Journal of Lightwave Technology, vol. 9, pp. 1124-1131, 1991
[24] R. D. Esman, M. Y. Frankel, J. L. Dexter, L. Goldberg, M. G. Parent, D. Stilwell, D. G. Cooper, IEEE Photonics Technology Letter, vol. 11, pp. 1347-1349, 1993
[25] R. Soref, Appl. Opt. Vol. 31, pp. 7395-7397, 1992
[26] Y. Chen, R. T. Chen, IEEE Photonics Technology Letters, vol. 14, pp. 1175 – 1177, 2002
[27] S. Yegnanarayanan, B. Jalali, IEEE Photonics Technology Letters, vol. 12, pp. 1049 – 1051, 2000
[28] L. P. Shen, W. P. Huang, G. X. Chen, S. S. Jian, IEEE Photonics Technology Letter, vol. 15, pp. 540-542, 2003
[29] A. Bjarklev, J. Broeng, A. Bjarklev, "Photonic Crystal Fibres", ISBN 1-4020-7610-X, Kluwer Academic Publishers, 2003
[30] P. St. J. Russell, Science, vol. 299, pp. 358-362, 2003
[31] J. A. West, N. Venkataramam, C. M. Smith, M. T. Gallagher, Proc. 27th Eur. Conf. on Opt. Comm. (ECOC '01), vol. 4, pp. 582 –585, 2001
[32] J. C. Knight, T. A. Birks, P. St. J. Russell, and D. M. Atkin, Optics Letters, Vol. 21, pp. 1547-1549, 1996
[33] T. A. Birks, D. Mogilevtsev, J. C. Knight, P. St. J. Russell, IEEE Photonics Technology Letters, vol. 11, pp. 674 – 676, 1999
[34] J. Broeng, S. E. Barkou, T. Sndergaard, A. Bjarklev, Opt. Lett., vol. 25, pp. 96-98, 2000
[35] A. Ferrando, E. Silvestre, J. J. Miret, P. Andrs, M. V. Andrs, Opt. Lett., vol. 24, pp. 276-278, 1999
[36] Y. Jiang, B. Howley, Z. Shi, Q. Zhou, R.T. Chen, M.Y. Chen, G. Brost, C. Lee, *IEEE Photonic Technology Letter*, Vol. 17(1): 187-189 (2005)
[37] Y. Jiang, Z.Shi, B. Howley, X. Chen, M. Y. Chen, R.T. Chen, *Optical Engineering*, vol. 44, No. 12, pp. 125001 (2005)
[38] Y. Jiang, W. Jiang, X. Chen, L. Gu, B. Howley, R. T. Chen, Proc. SPIE **5733**, 166 (2005)
[39] S. G. Johnson and J. D. Joannopoulos, Optics Express **8**, 173 (2001)
[40] B. Streetman, S. Banerjee, *Solid State Electronic Devices*, Prentice Hall (1999)
[41] M. Zelsmann, E. Picard, T. Charvolin, et al, J. Appl. Phys. **95**, 1606 (2004)